CHESAPEAKE BAY PLUME DYNAMICS FROM LANDSAT[1]

John C. Munday, Jr. and Michael S. Fedosh
Remote Sensing Center
School of Marine Science
College of William and Mary
Gloucester Point, Virginia

ABSTRACT

Examination of 81 dates of Landsat images with enhancement and density slicing has shown that the Chesapeake Bay plume usually frequents the Virginia coast south of the Bay mouth. Southwestern (compared to northern) winds spread the plume easterly over a large area. Ebb tide images (compared to flood tide images) show a more dispersed plume. Flooding waters produce high turbidity levels over the shallow northern portion of the Bay mouth.

INTRODUCTION

A central research question for the Atlantic marine fishery is the distribution of nutrients and pollutants outwelled from coastal bays and estuaries. Investigating the seaward flux of materials, both spatially and temporally, should be fruitful toward understanding fishery productivity and its fluctuations. The plume of the Chesapeake Bay, queen of the east coast estuaries, is attractive to study in this regard from several viewpoints (plume composition, volume discharge, Bay productivity, and Bay-shelf ecology), and has become the initial focus for flux studies coordinated by the NOAA National Marine Fisheries Service.

A leading phase of such study is to resolve the dynamics of the Chesapeake Bay plume. To do so by ship-based study alone would involve prohibitively large effort over long times; therefore, it is advantageous to use remote sensing technology provided by NASA to reduce the effort and provide repetitive synoptic views over large areas. The most striking view is provided by the NASA Landsat satellite, which since its first launch in 1972 has produced over eighty cloud-free images of the lower Chesapeake Bay region. The limitations of Landsat for Bay plume study are recognized -- the sensors primarily discriminate suspended sediment in the upper few metres of the water column, and the

images are only snapshots of continuous dynamic processes -- nevertheless, Landsat can provide an overview of the plume dynamics which is useful in guiding future aerial remote sensing and ship-based investigations.

In this study a large set of Landsat images has been examined using visual methods and image enhancement devices. The principal objective has been to determine what continental shelf regions are frequented by the Bay plume. A second objective has been to determine the effects of tidal phase and wind on plume dynamics.

METHODS

Eighty-one dates of cloud-free Landsat images of the southern Chesapeake Bay (path 15, row 34) were obtained from the USGS EROS Data Center, Sioux Falls, South Dakota. The overpass times span the phases of the diurnal tidal cycle as shown in Figure 1a; actual tide data were obtained for Sewells Point, Hampton Roads, which according to NOAA tidal tables experiences high and low tide 0:52 and 1:15 hours respectively after Cape Henry at the mouth of Chesapeake Bay. Tide data used in analysis of plume-tide relationships discussed later were adjusted for these differences. The distribution of dates over months of the year is shown in Figure 1b; surprisingly, there are no seasonal data gaps due to cloud cover. Seventy-five images are 18.5-cm (1:1,000,000) positive transparencies of MSS band 5; twenty dates (including six dates not studied in the large format images) were obtained in 70-mm-format (1:3,369,000) positive transparencies of MSS bands 4 to 7.
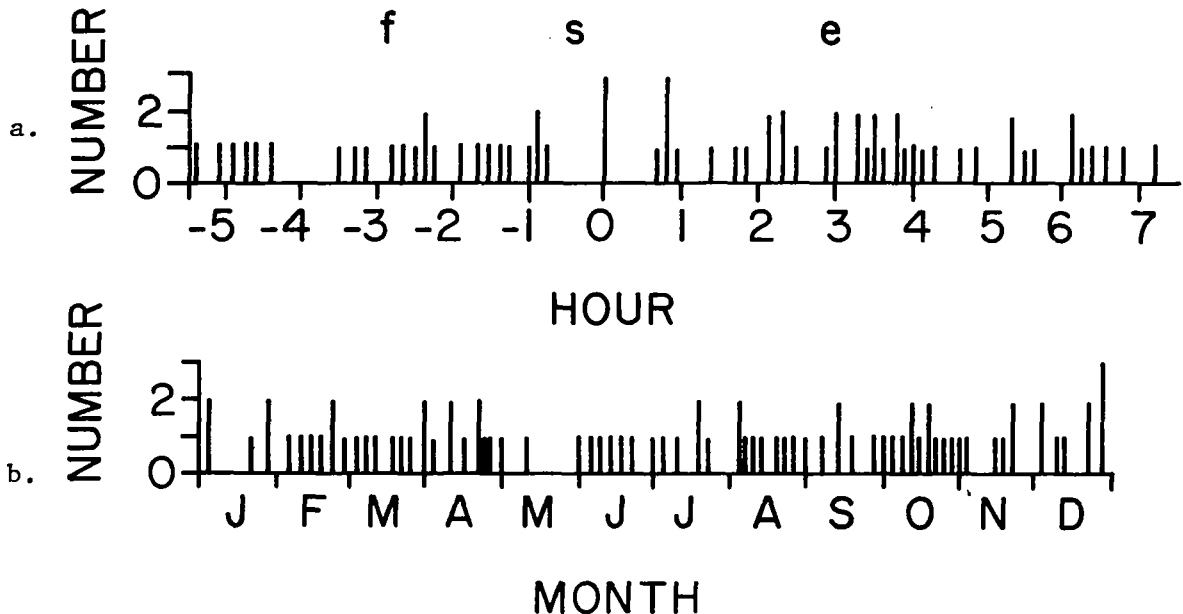

Figure 1. Tidal phases (1a:top) and seasonal distribution (1b:bottom) for Landsat overpasses of southern Chesapeake Bay. Tidal reference: high tide at Sewells Point, Hampton Roads.

Wind data were obtained from the Norfolk Regional Airport weather station covering the twelve hours preceding each overpass at 3-hour intervals. These data were vector-averaged for each pass; the composite wind regime for all passes is shown in Figure 2a, compared to the 1946-1970 record for Norfolk in Figure 2b. For use in image analysis the wind data of Figure 2a were grouped into the quadrants 0-89° (+0, 90, 180, and 270°) labeled 1, 2, 3, and 4.

The methods of image analysis included visual interpretation coupled with machine-assisted enhancement. Two interpreters analyzed each 18.5-cm image on a light table; the first interpreter traced turbidity boundaries manually based on visual inspection, and the second checked the tracing, making modifications as needed. The 70-mm images were enhanced with an International Imaging Systems (I^2S) color additive viewer, and the color enhancements were photographed on color slide (35-mm) film for projection during later analysis. Each 18.5-cm image was enhanced with an I^2S 32-channel optical density analyzer with a vidicon, digital processor, and color-coded television display. A black mask covering land areas was used during this analysis to focus attention on water patterns; that the mask had negligible effect on the density analysis was evidenced by the constancy of patterns when the image was rotated through 90°
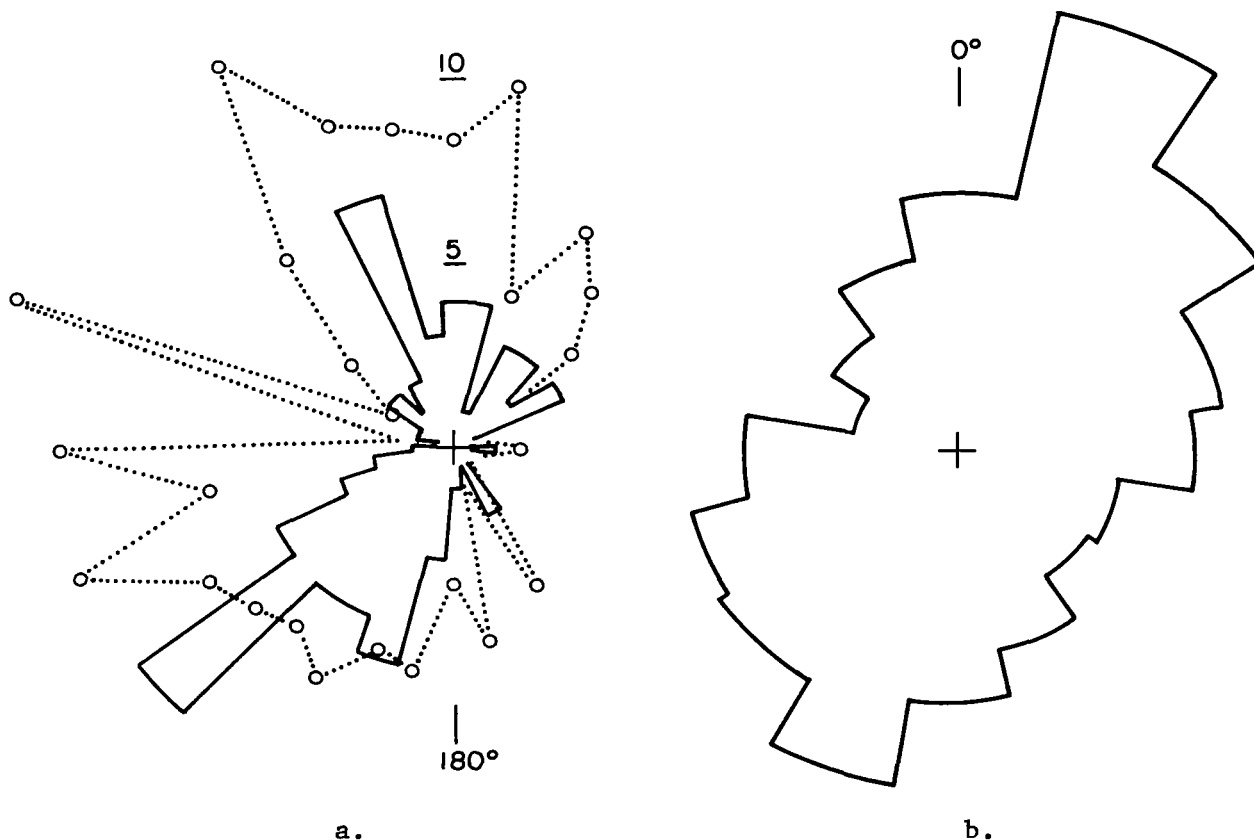

a.   b.

Figure 2. Winds at Norfolk Regional Airport.
   a. Landsat passes. Solid line: wind frequency. Dotted line: average wind speed in knots.
   b. The record for 1946-1970. Wind frequency only.

(the danger is that electronic band width limitations during scanning across sharp brightness gradients will cause smearing in the color coded output). The display was photographed on color slide (35-mm) film for projection during later analysis. Also, a contour map of optical density was prepared from the display by placing an acetate sheet on the I^{2}S light table and manually drawing contours while viewing the display monitor; this procedure produced contour maps at the original image scale.

The above procedures produced two types of maps. The one consists of visually-discriminated turbidity boundaries extending sometimes over long distances, possibly through background turbidity gradients not noticeable visually. These background gradients would be weak, because the eye during the mapping process ignores weak gradients, but enhances sharp gradients and emphasizes the continuity of turbidity-marked hydrodynamic features over long distances. The second type of map is of photographic density contours which qualitatively picture the absolute turbidity levels. With appropriate calibration this type of map could become a map of absolute concentrations of suspended solids.

In the contour map, a plume with a turbidity gradient will be dissected by the density contouring and may fail to be noticed. On the other hand, the I^{2}S is more sensitive than the eye to weak density changes, revealing turbidity boundaries which would not be detected by visual analysis alone. It is emphasized that visual maps and density contour maps enhance different aspects of an image and should not be expected to be similar. Examples of the maps are shown in Figure 3; negative copies of several 18.5-cm MSS 5 images (with masking of the land areas) are shown in Figure 4.

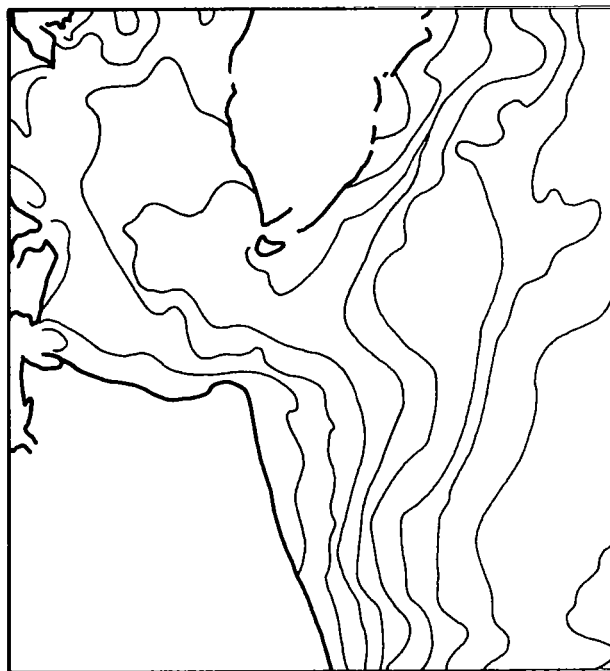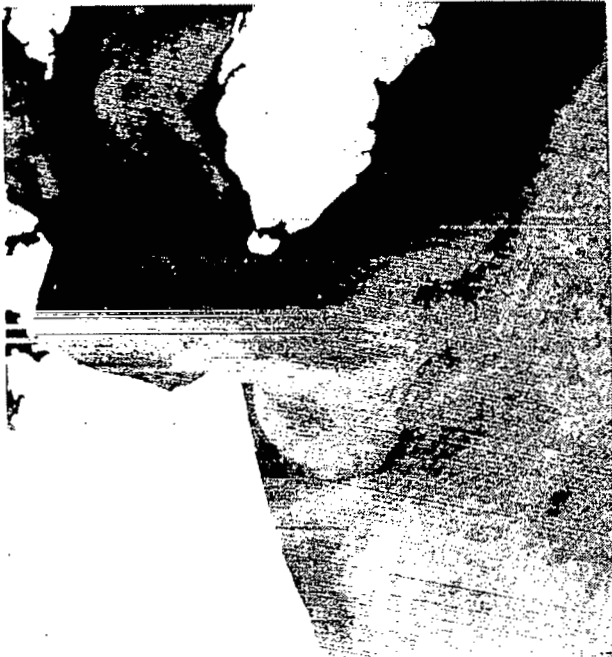Figure 3a. Visually discriminated turbidity boundaries for Landsat image of 8 July 1978.
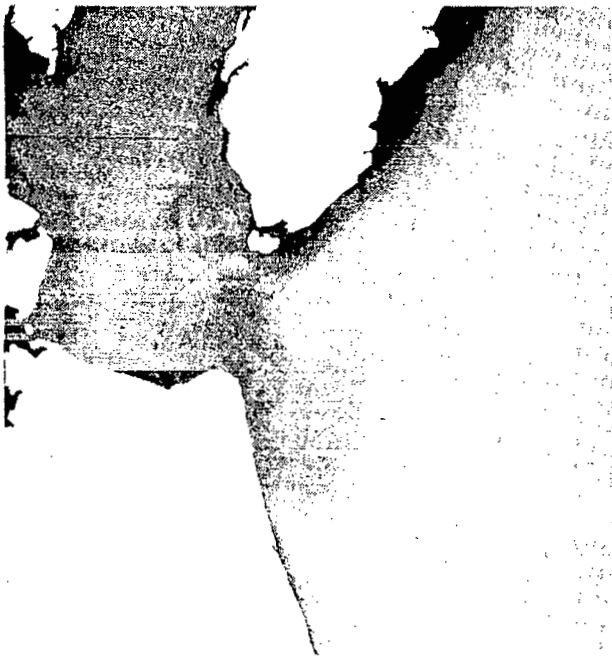
Figure 3b. Photographic density contours from density analyzer enhancement of same image.

4a. 27 Jan 78. -1:52; 251°, 19.6 kn.

4b. 13 Feb 73. +5:08; 217°, 4.2 kn.

4c. 19 Oct 79. +3:07; 60°, 1.9 kn.

4d. 11 Sep 77. +2:17; 354°, 9.9 kn.

Figure 4. Landsat images of the Chesapeake Bay plume. MSS 5 negatives with
masking of land areas. Top is north. Tides: hours before (-) or after (+)
high tide at Cape Henry. Winds: 12-hour average from Norfolk. Scale 1:10^6.

Patterns on the original 18.5-cm images and on the several data reduction products were simultaneously compared during extraction of measurements. Measurements were based on a 1-mm grid overlay (graph paper) facilitating use of the image scale of 1 mm:1 km. The distance and direction of plume-related features were measured with respect to an origin at 37° N latitude/76° W longitude. Azimuthal sectors and 1-cm grid squares frequented by turbid boundaries associated with the plume were determined using the sector and grid map in Figure 5; when an edge of the "plume" (see below) was noticed at some radial distance and direction from the origin, sector/zone segments radially outward to this position were "counted" (as having been "visited"). Simple relationships were then sought between the spatial distribution of counts and several variables including wind direction by quadrants (from 12-hour average wind vectors), wind speeds, wind duration, tidal phase, bathymetry, passage of weather fronts, and fresh water inflow into the Bay.

To the present, it has been possible to complete only some spatial analysis and statistical analysis using single-variable statistics. Further work is needed using multi-variate methods.
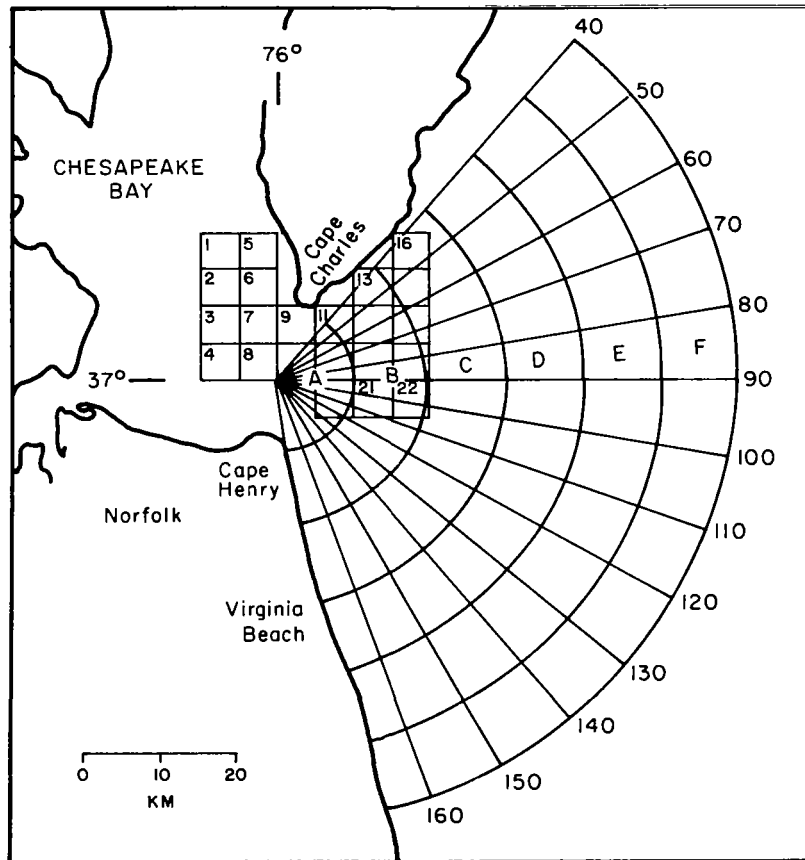

Figure 5. Sector and grid map for image data extraction.

DEFINITION OF THE "PLUME"

The counting of areas as "visited" was based only on the presence of turbidity discontinuities which appeared to be significant with respect to Chesapeake Bay plume dynamics. This counting policy was made deliberately wide and somewhat vague, because of the lack of historical data on plume dynamics. It gave the interpreters much freedom of choice. In subsequent studies, a more restrictive policy can be used based on the results obtained here.

There are several consequences of the above policy. First, some of the features of turbidity which were "counted" may be associated, not with the plume, but with along-shore currents. According to Bumpus (1973), there is generally a net non-tidal southerly current along the Eastern Shore and Virginia-North Carolina borders toward Cape Hatteras. This current could involve shear and turbidity gradients (some images give the impression of turbidity discontinuities parallel to shore at the 30-m isobath). Second, studies by Harrison et al. (1967), Johnson (1976), and Ruzecki et al. (1976) show that flow adjacent to Cape Henry is rotary, that the general southerly flow is sporadic rather than continuous, and that flow is wind-influenced in the along-shore direction. These findings should be considered in the interpretation of any observed features.

Third, it is probable that the collection of plume features on any one image is derived from several tidal cycles. In this regard, the distance of features from the mouth should be helpful in discriminating the different cycles. Drogue data published by Johnson (1976) and Ruzecki et al. (1976) suggest that the tidal excursion at the Bay mouth is only about 8 km, whereas at the Chesapeake Light Station (23 km east) the tidal excursion is negligible. Thus, features beyond 15-20 km almost certainly result from non-tidal flow and the net movement from several cycles of tidal flow.

However, apart from the distance factor, the features themselves do not suggest a distinction between features for the cycle in progress from those for preceding cycles. Distinguishing sequential plumes using multispectral satellite images was first described by Mairs and Clark (1973); their approach was not successful here because plumes are too faint on the small set of multispectral images on hand. Defining plumes more clearly using digital processing of Landsat CCT data should prove useful. In contrast, for the smaller plumes from the Eastern Shore inlets, the distinction of sequential tidal cycles is possible on single band images; the inlet plumes often have the appearance of a sequence of turbidity pulses.

Fourth, it should be noted that Landsat records upwelling radiance from only the surface layers. The depth of the observed turbidity varies inversely with its opacity, with the depth of observation for prevailing turbidities being perhaps 5 m. Thus, plume features at greater depth are not recorded. Also, higher turbidities are produced by scour and resuspension over shallow depths, with the consequence that turbidity levels become decoupled from plume waters per se. Generally, then, Landsat is not always recording plume water boundaries as defined by vertical profiles of temperature, salinity, nutrients and biological variables.

Composites of Observed Boundaries

Composites of the turbid boundaries seen on all the images divided into flood and ebb tide groups are shown in Figure 6. Viewed in the manner of a geologic fault map, the ebb tide composite shows most "lineaments" found between Cape Charles and Cape Henry are oriented toward 120°. The flood tide lineaments although more random are oriented similarly. In both cases, most lineaments beyond the mouth are found near the coast southward; only a few lineaments beyond the mouth are found toward 40° to 90°. An initial hypothesis was therefore that the plume usually frequents the southeasterly direction. Subsequent analysis was oriented toward testing this hypothesis.


Figure 6a. Composite of turbidity boundaries for flood tide.

Figure 6b. Composite of turbidity boundaries for ebb tide.
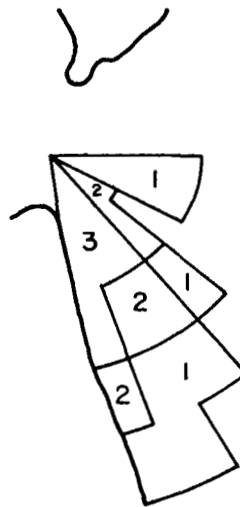
Sector/Zone Count Analyses

The map in Figure 7a shows sector/zone counts for all wind classes and tidal phases; zones A through E for sectors at $\theta \sim 150°$ are the most frequently visited. Sorting the pass dates by wind quadrant, Q_i, yields $Q_1 = 20$ images, $Q_2 = 3$, $Q_3 = 41$, $Q_4 = 17$. Maps for the wind quadrants are shown in Figures 7b-d (a map is omitted for Q_2 because of its low value). Q_4 produced the tightest pattern along the Virginia-North Carolina coast; Q_3 (southwest winds) produced the most dispersed pattern (notice especially the visits to zones D-F for $\theta \sim 90°$).
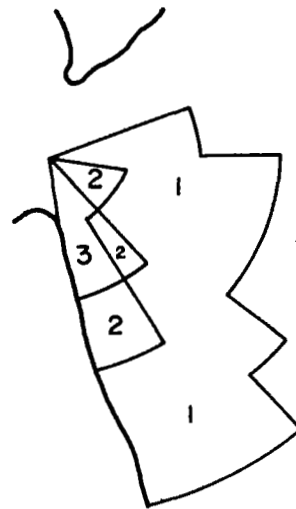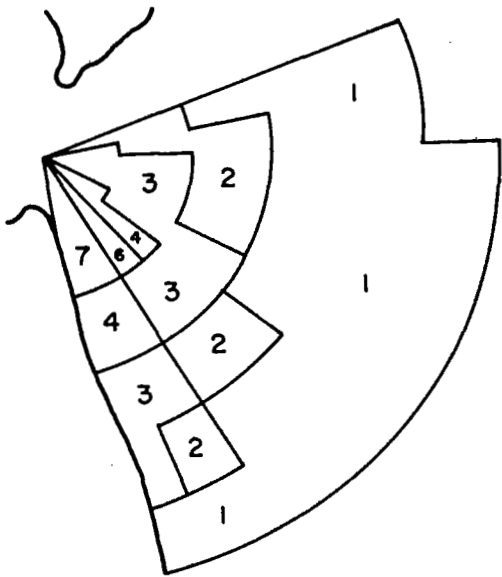
a. All wind quadrants.

b. Winds from quadrant 1: 0°-90°.
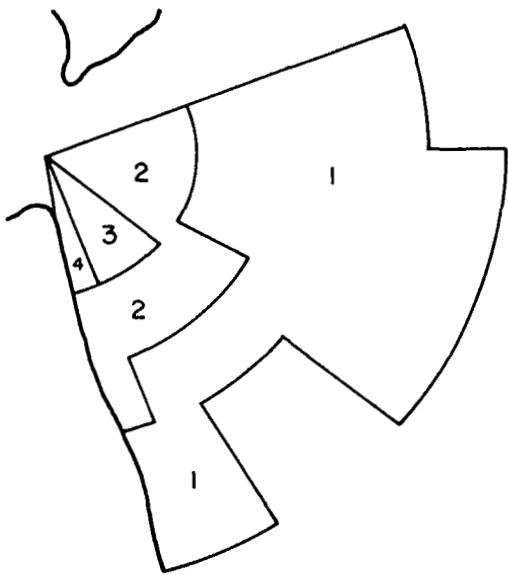
c. Winds from quadrant 3: 180°-270°.

d. Winds from quadrant 4: 270°-360°.

Figure 7. Areas visited by the plume under different wind conditions. The numerals represent sector/zone counts as follows: 1: 0-5 counts; 2: 6-10; 3: 11-20; 4: 21-30; 5: 31-40; 6: 41-50; 7: >50.

To enhance the differences between results from different wind quadrants, ratios have been formed of sector/zone counts using the quadrants 3 over 1, and 4 over 1. Counts for each quadrant were adjusted upward by 1 count for each pass where no plume was discriminated (which in effect produces a contrast stretching of the ratios): the adjustment frequencies for each quadrant were 1, 1, 6, and 0 respectively. The ratios were then normalized for differences among the Q_i values. The resulting ratios R are shown in Tables 1 and 2. Numerical values of R near 1.0 indicate no difference in effects of wind direction for the two quadrants under consideration. Table 1 (quadrants 3 over 1) shows R >1 for $\theta < 140°$ (zones B-E), a clear demonstration that southwest (compared to northeast) winds disperse the plume over a larger area and swing its dominant direction away from the southeast toward the east. Table 2 (quadrants 4 over 1) demonstrates that northwest (compared to northeast) winds constrain the plume to the coastline toward the southeast.

TABLE 1

NORMALIZED RATIOS OF COUNTS

FOR WIND QUADRANT 3 OVER QUADRANT 1

Zone / Sector	6*	7	8	9	10	11	12	13	14	15	16
A	1.46	1.46	1.46	1.27	0.91	0.98	1.12	0.92	0.77	0.83	0.84
B	∞	2.93	1.95	2.44	1.83	1.83	1.95	1.66	1.25	0.84	0.88
C	3.41	4.39	4.88	2.68	1.79	1.34	2.11	1.71	0.98	0.80	0.98
D	3.90	3.90	4.39	4.39	3.90	4.39	4.39	2.44	1.46	0.98	0.98
E	2.93	3.41	3.41	3.41	3.41	3.41	3.41	2.93	1.46	1.30	1.22

TABLE 2

NORMALIZED RATIOS OF COUNTS

FOR WIND QUADRANT 4 OVER QUADRANT 1

Zone / Sector	6*	7	8	9	10	11	12	13	14	15	16
A	0	0	0	0.24	0.17	0.34	1.01	1.18	1.01	1.09	1.02
B		0	0	0.39	0.29	0.29	0	1.88	1.57	1.02	1.02
C				0	0	0	0	0.29	1.18	1.32	1.62
D								0	0.39	0.94	1.18
E									0	0.39	0.29

* 10° interval from 60° to 70°; similarly for all sectors.

Sector-count maps for flood versus ebb tide in Figure 8 show somewhat more dispersion of plume features for ebb tide. A subset of the ebb tide data for southwest winds (Q3) higher than 8 knots included only five images; in these images a plume could not be discriminated. These results are further evidence that southwest winds disperse the plume on ebb tide.

In subsequent study, polar coordinates were determined for the most distant point on each plume. The results for flood and ebb tides and wind quadrants Q1, Q3, and Q4 are shown in Figure 9a through 9f. The results are similar to the earlier results. The results show that southwestern winds for passes during ebb tide are associated with the greatest dispersion and extension of the plume. For northern winds, plumes for all tidal phases are found close to Virginia Beach.
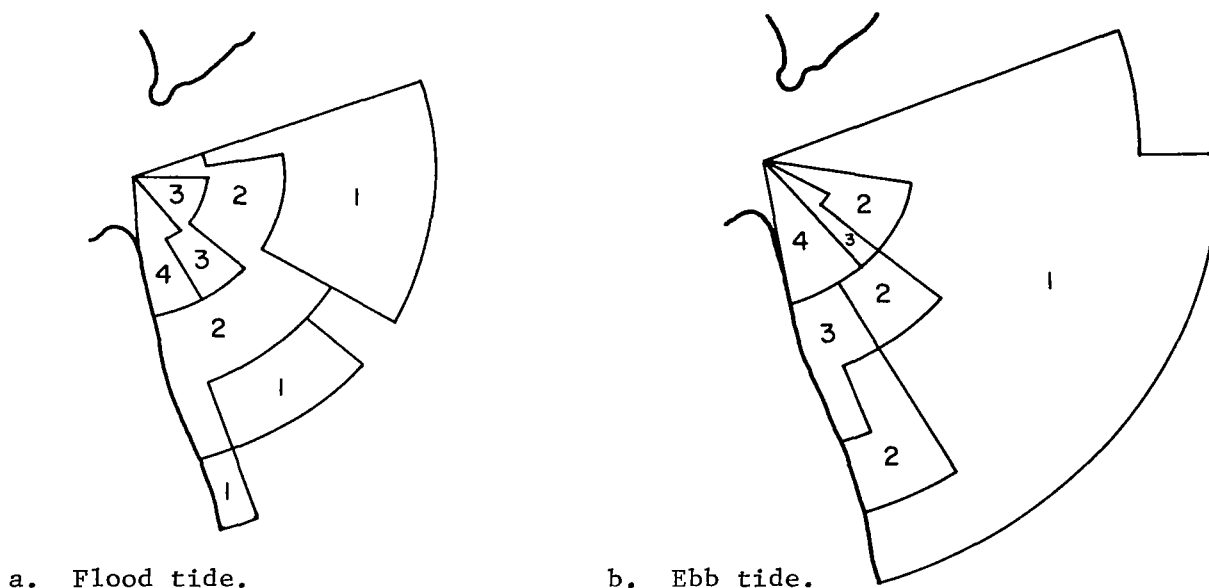

a. Flood tide.   b. Ebb tide.

Figure 8. Areas visited by the plume under different tidal phases. Same numerical symbols as in Figure 7.

Cape Charles Grid Analysis

Many images reveal turbidity in late-ebb/early-flood, located adjacent to Fisherman's Island (at the tip of Cape Charles) on the north side of the Bay mouth (Munday and Fedosh, 1980). The patterns suggest that early flood waters moving into the northern side of the Bay mouth carry residual suspended sediment from the Eastern Shore nearshore zone, and additional material resuspended in the shallow areas adjacent to Fisherman's Island. If true, turbidity on the western side of the mouth (compared to the eastern side) should be relatively more frequent during flood, as flooding waters traverse increasing areas of shallows.

a. Flood; 0°-90°.   b. Flood; 180°-270°.   c. Flood; 270°-360°.

d. Ebb; 0°-90°.   e. Ebb; 180°-270°.   f. Ebb; 270°-360°.
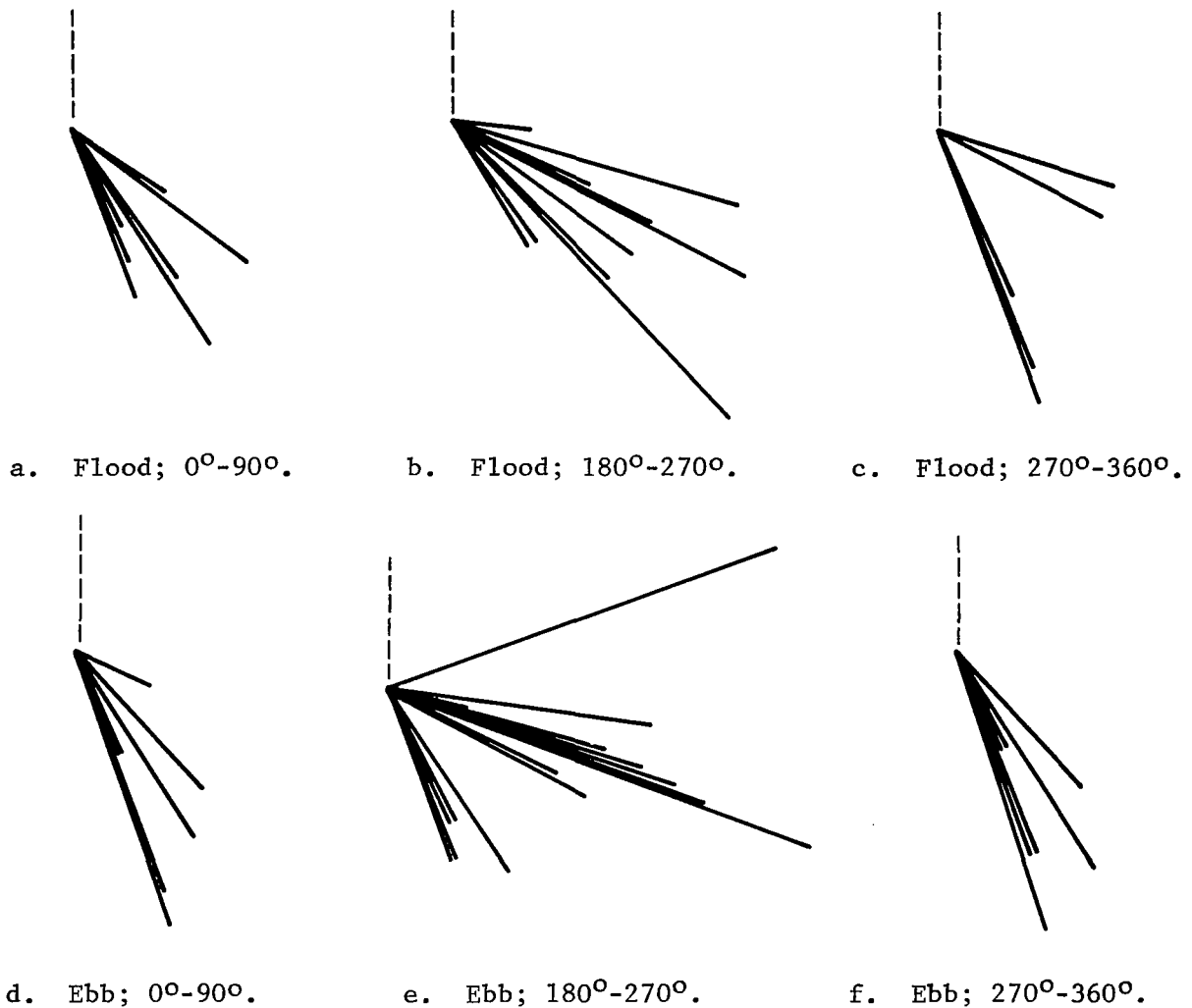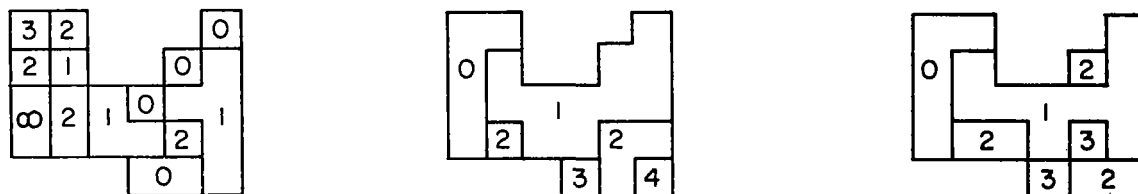
Figure 9. Plume extension under different tidal and wind conditions. Radial lines for the most distant point on each plume. North shown as dotted line.

To test this hypothesis quantitatively using Landsat images, a counting procedure was employed based on the square grid shown in Figure 5. A cell was counted when turbidity in the cell was higher than background as judged visually. Counts were made for ebb and flood tide passes and subset into the four wind quadrants. Ratios of flood to ebb counts were formed and normalized for flood and ebb pass frequencies; the normalized ratios truncated to integers are shown in Figure 10a. Western cells are, as expected, relatively more frequented by turbidity than eastern cells during flood tide. Truncated normalized ratios for the wind quadrants are shown in Figure 10b for Q_1 over Q_3, and Figure 10c for Q_1 over Q_4 (Figure 10c numbers were multiplied by 2 before plotting). Figures 10b and 10c demonstrate that western (compared to northeastern) winds reduce western and increase eastern turbidities.

90

Figure a: Flood/ebb ratios grid: 3 2 ... 0 / 2 1 ... 0 / ∞ 2 1 0 ... 1 / 2 / 0

Figure b: Wind quadrants 1 to 3 grid: 0 / 1 / 2 ... 2 / 3 4

Figure c: Wind quadrants 1 to 4 grid: 0 / ... 2 / 1 / 2 ... 3 / 3 2

a. Flood/ebb ratios.   b. Wind quadrants 1 to 3.   c. Wind quadrants 1 to 4 (ratios x 2).

Figure 10. Relative turbidity near Cape Charles. Frequency ratio for each grid cell normalized and truncated.

Wind Duration and Wind Speed

Correlation and regression analyses have been performed on wind speed and wind duration versus plume extension, with tidal phase and wind quadrant as parameters. None of the analyses have yet produced statistically significant results. Multivariate statistical methods will be utilized for further analysis. Perhaps appropriate measures of the plume have yet to be discovered.

DISCUSSION

Image analysis has shown that the "plume" (as broadly defined here) usually frequents the southeasterly direction (120°-150° relative to the mouth). Passes during ebb (compared to flood) show a somewhat more dispersed plume. Southwestern winds are effective in dispersing and extending the plume, especially on ebb tide passes, while for northern winds plumes remain close to Virginia Beach.

These effects of winds have been shown using vector-averaged Norfolk wind data from the 12 hours preceding the Landsat overpass. Because the shelf water relaxation time from wind effects is probably greater than 12 hours, longer wind records should be studied. Also, Chesapeake Light Tower winds would perhaps be more appropriate than Norfolk winds for examining the effect of shelf water currents on the plume dynamics.

For flood tide, a striking feature of many images is a strong turbidity pattern on the shallow northern side of the Bay mouth adjacent to Fisherman's Island. The pattern suggests a predominance of the northern side during flood tide, due to the Coriolis force and southerly drift along the Eastern Shore. Analysis shows that the turbidity is relatively greater in flood tide and northeastern winds. No such patterns were observed for flood tide in the southern portion of the Bay mouth; in addition to the Coriolis deflection toward the north, the water in the southern portion is much deeper, reducing surface turbidities which originate in tidal scour.

For ebb tide, the plume for northerly winds is tongue-shaped, but the shape is difficult to characterize further. Little was observed which would suggest rotary motion off Cape Henry as observed by Harrison et al. (1967).

REFERENCES

Bumpus, D.F. 1973. A description of the circulation on the continental shelf of the east coast of the United States. Progress in Oceanography (Ed. B.F. Warren), 6:111-156. Pergamon Press, N.Y.

Harrison, W., J.J. Norcross, N.A. Pore, and E.M. Stanley. 1967. Circulation of shelf waters off the Chesapeake Bight. ESSA Prof. Paper No. 3, U.S. Dept. Commerce, Washington, D.C., 82 p.

Johnson, R.E. 1976. Circulation study near Cape Henry, Virginia, using Lagrangian techniques. Techn. Rep. No. 21, Inst. Oceanography, Old Dominion Univ., Norfolk, Virginia, 80 p. + app.

Mairs, R.L. and D.K. Clark. 1973. Remote sensing of estuarine circulation dynamics. Photogramm. Eng. 39(9):927-938.

Munday, J.C., Jr. and M.S. Fedosh. 1980. Southern Chesapeake Bay circulation and suspended sediment transport analyzed using Landsat imagery. Proc. Amer. Soc. Photogr. Fall Techn. Mtg., Niagara Falls, N.Y., p. RS3F:1-5.

Ruzecki, E.P., C. Welch, J. Usry, and J. Wallace. 1976. The use of the EOLE satellite system to observe continental shelf circulation. Eighth Ann. Offshore Techn. Conf., Houston, Texas, p. 697-708.